

Ion-implantation-enhanced chalcogenide-glass resistive-switching devices

Mark A. Hughes^{*}, Yanina Fedorenko, Russell M. Gwilliam, Kevin P. Homewood, Steven Hinder, Behrad Gholipour, Daniel W. Hewak, Tae-Hoon Lee, Stephen R. Elliott, and Richard J. Curry

Citation: *Appl. Phys. Lett.* **105**, 083506 (2014); doi: 10.1063/1.4894245

View online: <http://dx.doi.org/10.1063/1.4894245>

View Table of Contents: <http://aip.scitation.org/toc/apl/105/8>

Published by the [American Institute of Physics](#)



**FIND THE NEEDLE IN THE
HIRING HAYSTACK**

POST JOBS AND REACH THOUSANDS OF
QUALIFIED SCIENTISTS EACH MONTH.

PHYSICS TODAY | JOBS
WWW.PHYSICSTODAY.ORG/JOBS

Ion-implantation-enhanced chalcogenide-glass resistive-switching devices

Mark A. Hughes,^{1,a)} Yanina Fedorenko,¹ Russell M. Gwilliam,¹ Kevin P. Homewood,¹ Steven Hinder,² Behrad Gholipour,³ Daniel W. Hewak,³ Tae-Hoon Lee,⁴ Stephen R. Elliott,⁴ and Richard J. Curry¹

¹*Department of Electronic Engineering, Advanced Technology Institute, University of Surrey, Guildford GU2 7XH, United Kingdom*

²*The Surface Analysis Laboratory, Department of Mechanical Engineering, University of Surrey, Guildford GU2 7XH, United Kingdom*

³*Optoelectronics Research Centre, University of Southampton, Southampton SO17 1BJ, United Kingdom*

⁴*Department of Chemistry, University of Cambridge, Lensfield Road, Cambridge CB2 1EW, United Kingdom*

(Received 26 May 2014; accepted 6 August 2014; published online 27 August 2014)

We report amorphous GaLaSO-based resistive switching devices, with and without Pb-implantation before deposition of an Al active electrode, which switch due to deposition and dissolution of Al metal filaments. The devices set at 2–3 and 3–4 V with resistance ratios of 6×10^4 and 3×10^9 for the unimplanted and Pb-implanted devices, respectively. The devices reset under positive Al electrode bias, and Al diffused 40 nm further into GaLaSO in the unimplanted device. We attribute the positive reset and higher set bias, compared to devices using Ag or Cu active electrodes, to the greater propensity of Al to oxidise. © 2014 AIP Publishing LLC.

[<http://dx.doi.org/10.1063/1.4894245>]

Resistive switching is a feature of a recently discovered¹ circuit element, the memristor, in which its resistance depends on the current that has previously flowed through the element. Resistive switching has been observed in various material systems, including organic films,² where switching has been attributed to the formation of metal filaments or chains of nanoparticles, and metal oxides, especially TiO₂,³ where switching is attributed to the drift of positively charged oxygen vacancies. Chalcogenide glasses are well known for their propensity to permit the diffusion of various metal ions.⁴ This phenomenon has been exploited to fabricate resistive switching devices, known as electrochemical metallization (ECM) cells, where switching between a low resistive (on) state and a high resistive (off) state is achieved through the transport of metal ions from an active electrode to an inactive electrode through a chalcogenide glass film.⁵ Commonly used chalcogenide glasses for this purpose include GeSbTe,^{6,7} As₂S₃,⁸ GeSe,^{7,9,10} GeTe,¹¹ AgGeSe,⁵ and AgGeS.¹² All these devices use Ag or Cu as an active electrode. GaLaSO is a non-standard chalcogenide material, which has not, until now, been exploited for resistive switching devices. GaLaSO has a resistivity over ten orders of magnitude greater than GeSbTe, making it potentially more suitable for the high off-state resistances required in mobile-communication power-supply application devices, where the standby time could be increased.¹³ It could also be more suitable for the high resistance ratios required for field-programmable gate array (FPGA) applications.⁶ Resistive switching devices also have applications in non-volatile memory, where, compared to flash and chalcogenide phase-change memory, they could offer lower power consumption, faster switching speed, and higher density.^{14–16} Furthermore, resistive switching devices could form the synapses in solid-state neuromorphic circuits.¹⁷ The large atomic weight of Pb means its implantation should cause significant modification

of GaLaSO structure. In this work, we report GaLaSO-based resistive switching devices in which the resistance ratio improved from 6×10^4 to 3×10^9 with the implantation of Pb before the deposition of an Al active electrode.

We fabricated resistive switching devices by sputtering 230 nm of GaLaSO onto a 100 nm InSnO (ITO)-coated borosilicate glass substrate, before sputtering 100 nm thick Al top contacts through a shadow mask with circular 500 μm diameter holes. A second set of devices was fabricated concurrently, but implanted with Pb with a dose of 3×10^{15} ions/cm² and an energy of 350 keV before deposition of Al top contacts. Transport of Ions in Matter (TRIM) software simulations indicated this was the maximum dose to give <10 nm of sputtering. We used ITO as an inactive bottom electrode because this conductive oxide layer should have minimal diffusion of metal ions compared to the metallic active top electrode. The device schematic is illustrated in Figure 1(a). The thickness of the layers is confirmed in the SEM cross section in Figure 1(b). The sputtering target fabrication, ion-implantation procedure, and Rutherford back-scattering (RBS) measurements have been described previously,¹⁸ as have the IV measurements setup¹⁹ (bias was applied to the Al top electrode) and time-of-flight secondary ion mass spectrometry (ToF-SIMS)²⁰ (using a Cs ion beam etch). SEM cross sections were taken on a FEI Nova NanoLab DualBeam SEM/FIB and obtained by depositing a protective Pt layer, then etching with a Ga focused ion beam (FIB). Cryogenic measurements were taken by placing the device in a liquid nitrogen cryostat.

In order to characterise the GaLaSO film itself, we sputtered 100 nm of GaLaSO onto a 1 μm thick thermally oxidized SiO₂ on Si substrate, then implanted with Pb at 3×10^{15} ions/cm². The resistance of the film was measured by taking two probe IV scans across the films. Resistivity vs temperature for Pb-implanted and unimplanted films are shown in Figure 1(c). It shows that the Pb implant causes no change in the resistivity of the film. Sputter markers indicated

^{a)}Electronic mail: m.a.hughes@surrey.ac.uk

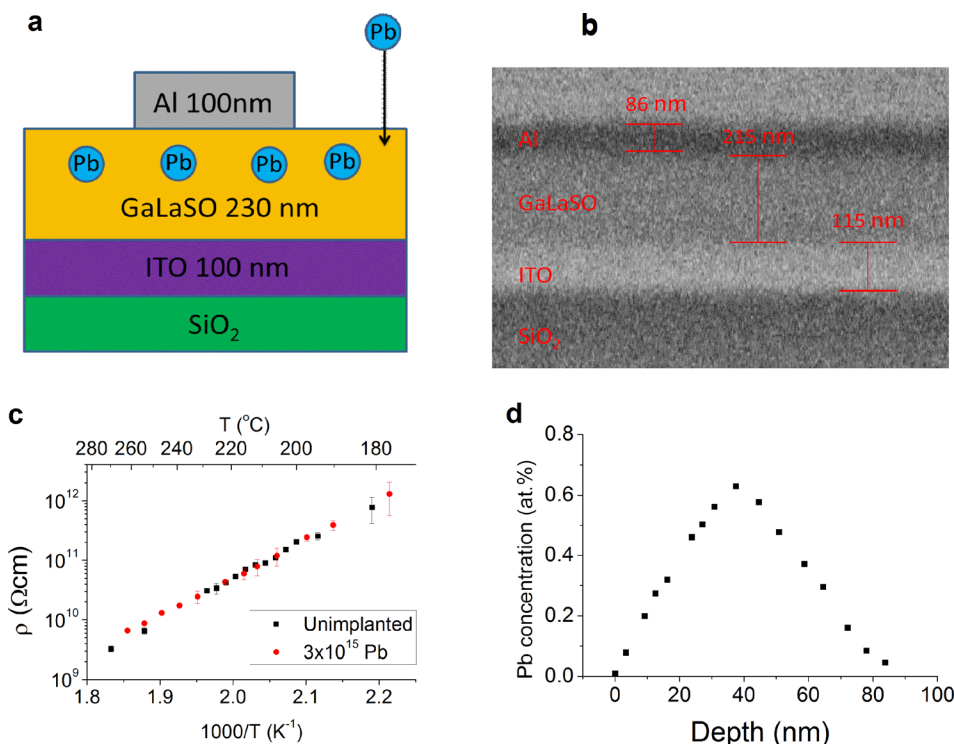


FIG. 1. (a) Schematic of the device structure, showing the nominal thicknesses of the layers. One set of devices had a 3×10^{15} ions/cm² Pb-implant prior to deposition of the Al top contact; another set had no implantation stage. (b) SEM cross section of a Pb-implanted device showing the measured thickness of each layer. (c) Resistivity vs temperature for 3×10^{15} ions/cm² Pb-implanted and unimplanted 100 nm thick GaLaSO film (unannealed). (d) Depth profile of Pb in a 3×10^{15} ions/cm² Pb-implanted GaLaSO film measured by RBS. The RBS measured film composition was Ga₂₆La₁₂S₄₅O₁₇; the measured Pb dose was 3.1×10^{15} ions/cm².

that no sputtering of the GaLaSO film occurred after implantation. At temperatures below 180 °C, the resistance was above the measurement system limit. GeSbTe has a resistivity of 16 Ωcm at 140 °C;²¹ above this temperature, it crystallizes. Figure 1(c) shows that GaLaSO has a resistivity of 1×10^{12} Ωcm at 180 °C. Therefore, GaLaSO will have a resistivity over ten orders of magnitude greater than GeSbTe at 140 °C. RBS measurements in Figure 1(d) show the implanted Pb has a peak concentration of 0.6 at. % at 40 nm.

Room-temperature IV measurements of the unimplanted and Pb-implanted devices are shown in Figures 2(a)

and 2(b), respectively. Both devices show set-reset behaviour, with the unimplanted device setting at 2–3 V and resetting at ~0.2 V, and the Pb-implanted device setting at 3–4 V and resetting at ~1 V. We found that the highest resistance ratio was achieved when sweeping from –3 to +5 V. The IV curves are shown on the same scale; comparison shows that the Pb-implanted device has a significantly higher on-state current (1×10^{-4} A vs 1×10^{-7} A) and lower off-state current (1×10^{-15} A vs 1×10^{-11} A) than the unimplanted device. The higher on-state current cannot be due to an increased conductivity of GaLaSO because the conductivity

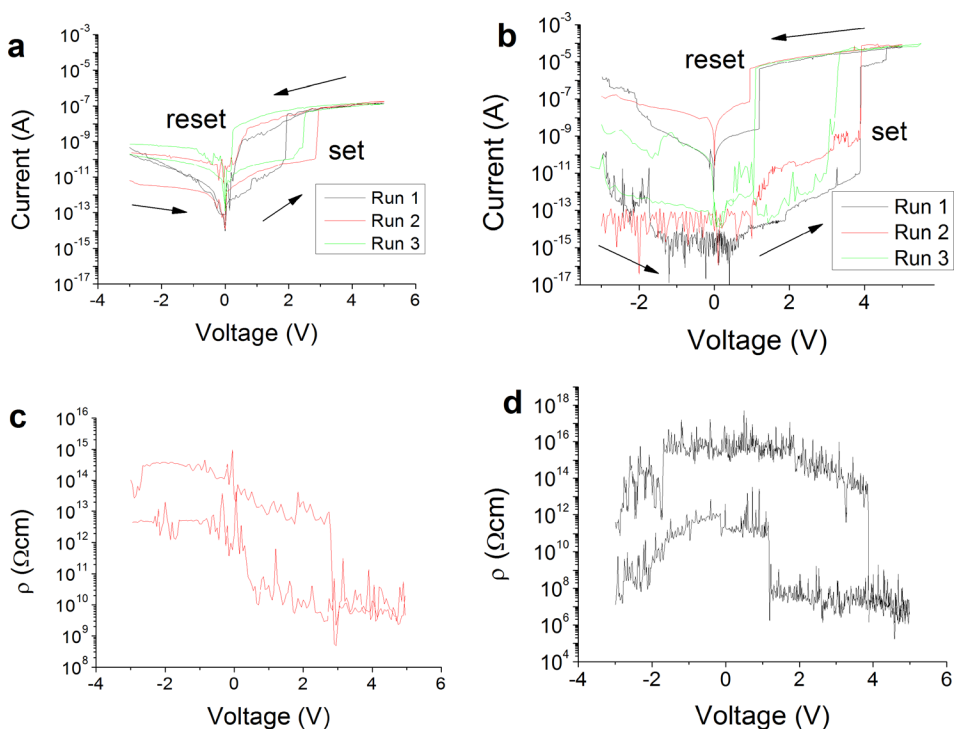


FIG. 2. (a) Three consecutive runs of absolute current vs voltage of the unimplanted device. (b) Three consecutive runs of absolute current vs voltage of a 3×10^{15} ions/cm² Pb-implanted device. (c) Resistivity vs voltage of run 2 of the unimplanted device. (d) Resistivity vs voltage of run 1 of the Pb-implanted device. All measurements were at room temperature.

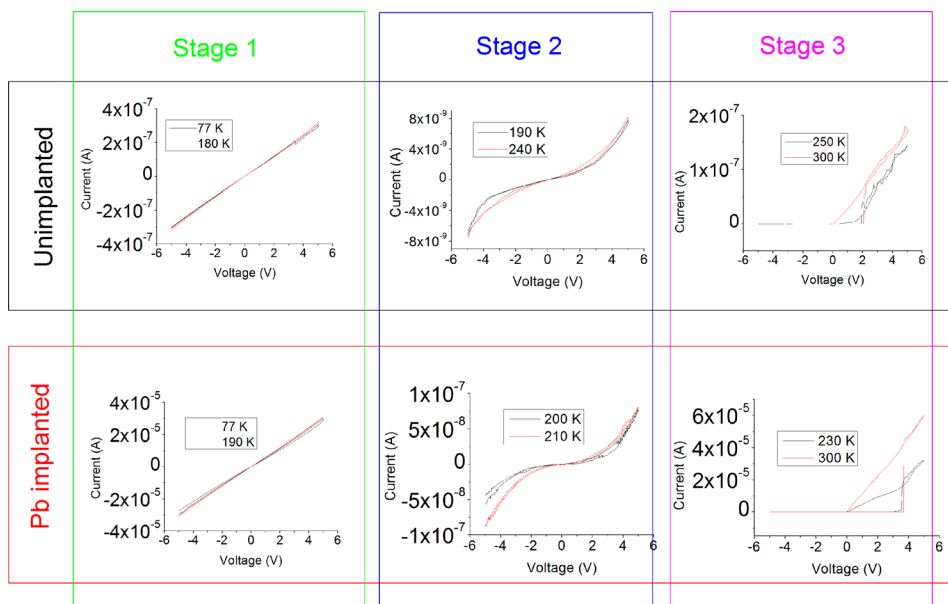


FIG. 3. IV measurements at temperatures between 77 and 300 K for an unimplanted and Pb-implanted device. Three distinctive forms of IV curves (stages 1–3) could be observed as the temperature was increased from 77 to 300 K.

measurements in Figure 1(c) show that Pb implantation does not increase the conductivity of GaLaSO; it must therefore be due to differences in the dynamics of Al-ion diffusion caused by Pb implantation. Device resistivity vs voltage was obtained from dI/dV data. Figures 2(c) and 2(d) show the resistivity vs voltage of the highest resistance ratio run from the unimplanted and Pb-implanted devices, respectively. Figure 2(c) shows that the unimplanted device has a resistance ratio of 6×10^4 , and Figure 2(d) shows that the Pb-implanted device has a resistance ratio of 3×10^9 .

Cryogenic IV measurements presented in Figure 3 show that, when Pb-implanted and unimplanted devices are cooled to 77 K, the devices behave as almost ideal ohmic conductors with resistivities of $7 \times 10^7 \Omega \text{cm}$ and $6 \times 10^9 \Omega \text{cm}$, respectively; these resistivities are similar to the low-resistance states of these devices when they show bi-stable switching at room temperature. The resistivity changes little as the temperature is increased to 180 K for the unimplanted sample, and 190 K for the Pb-implanted device (stage 1), indicating hopping or metallic conduction. Above these temperatures, the devices convert to a higher resistance state with non-ohmic conduction (stage 2). As the temperature is increased above 240 and 210 K for the unimplanted and Pb-implanted devices, respectively, the devices revert to the bi-stable switching behaviour observed at room temperature (stage 3). This indicates that the resistive switching behaviour is a thermally activated process. Capacitance-voltage (CV) measurements at 10 kHz were largely featureless, indicating that the effect of interface states is minimal.

Figure 4 shows the Al signal from ToF-SIMS measurements of the unimplanted and Pb-implanted devices. The Al top electrode is clearly evident as a high Al count through the first 4000 s of etching. The count then drops to baseline in the GaLaSO layer, then increases slightly at the ITO interface, presumably due to Al impurities in the ITO. Importantly, there are clear differences in how the Al signal decreases in the GaLaSO layer between the unimplanted and Pb-implanted devices. The Al/GaLaSO interface should be where the rate of Al signal decrease is at its maximum. In the Pb-implanted device, the Al signal decreases at a

relatively low rate immediately after the Al/GaLaSO interface; however, in the unimplanted device, the Al signal remains flat for about 20% of the etch time required for the entire GaLaSO layer, equivalent to about 40 nm, before decreasing in the same manner as the Pb-implanted device. This indicates that Al ions from the top electrode have diffused into the GaLaSO layer and that in the unimplanted device they penetrate 40 nm further than in the Pb-implanted device.

The switching mechanism proposed for chalcogenide ECM cells involves the electrochemical deposition and dissolution of conductive metal filaments during set and reset, respectively.⁵ Applying this switching mechanism to our devices, the application of a positive bias to the Al electrode should cause the dissolution of the Al into the GaLaSO, according to the reaction $\text{Al} \rightarrow \text{Al}^{z+} + z\text{e}^-$. The Al^{z+} ions are then transported across the GaLaSO film under the influence of a positive electric field and deposited at the ITO cathode according to the reaction $\text{Al}^{z+} + z\text{e}^- \rightarrow \text{Al}$; when a conductive Al filament bridges the electrodes, the device is set. The observation in Figures 2 and 3 that switching only occurs when a positive bias is applied to the Al electrode indicates that

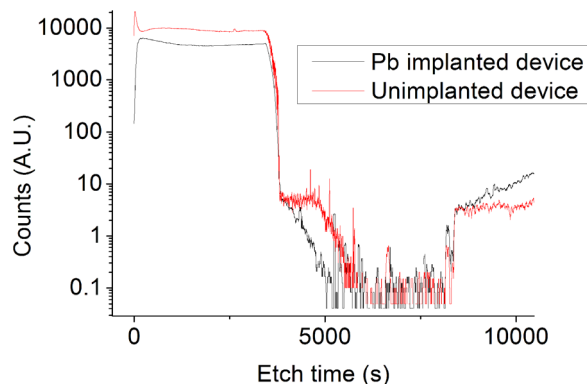


FIG. 4. ToF-SIMS data showing the Al signal as a function of etch time from an unimplanted and Pb-implanted device. The devices were both left in an off-state before the ToF-SIMS measurements.

electrochemical transport of ions from the Al electrode only is occurring. The device should reset due to dissolution of the conductive filaments under the influence of a negative electric field, according to the reaction: $\text{Al} \rightarrow \text{Al}^{z+} + z\text{e}^-$. The positive reset bias that we can observe in Figure 2(b) can be explained by the negative reduction potential of Al, which would give Al metal filaments a propensity to oxidise. Figure 3 shows that our devices are in an on-state at cryogenic temperatures, then in an off-state at higher temperatures; this indicates that there is a different temperature dependence for the deposition and dissolution reactions. So, at stage 1, the deposition reaction dominates and the device is permanently in an on-state. At stage 2, the dissolution reaction dominates so the device is permanently in an off-state. At stage 3, both the deposition and dissolution reactions can occur and bi-stable switching occurs.

ECM devices without doping in the chalcogenide layer often require an electroforming voltage before bi-stable switching can be observed.⁵ This electroforming voltage is usually higher than the set voltage and is required to incorporate metal ions in the chalcogenide. Our virgin devices had IV curves that were similar to subsequent runs, indicating that no electroforming was required. Another mechanism for set-reset behaviour in resistive switching devices is the drift of positively charged oxygen vacancies under the applied electric field to form conductive channels.³ This mechanism is usually considered for transition metal oxide-based resistive-switching devices,³ but not for chalcogenide-based devices because of their lack of oxygen content. However, since the GaLaSO used in our device contains 17 at. % oxygen, it should be considered. The conductivity of SrTiO₃ thin films varies by several orders of magnitude as the oxygen partial pressure is reduced from ambient because of its effect on oxygen vacancies.²² We observed no variation in the conductivity of our devices when they were placed in an evacuated cryostat. In addition, the IV characteristics of resistive switching devices attributed to the oxygen-vacancy mechanism display a continuous change in current during the set and reset stages,^{3,23} rather than the abrupt change in current observed in our device and other chalcogenide-based devices attributed to the electrochemical-deposition mechanism.^{5–12} ToF-SIMS data in Figure 4 are for devices that have been cycled through many set-reset operations, yet they show no detectable Al throughout the majority of the GaLaSO film. This indicates that, after dissolution of Al filaments following the reset operation, Al^{z+} ions are deposited back at the Al electrode or are swept in close proximity to the Al electrode. The lack of an electroforming stage also indicates that there is little Al doping of the GaLaSO.

The high mobility of metal cations in the amorphous sulphides and oxides used in ECM systems is due to the long-range disorder in these materials and resulting fast-ion transport paths.⁵ The implantation of Pb into GaLaSO at a dose of 3×10^{15} ions/cm² should significantly increase the long-range disorder of the GaLaSO, which could increase the diffusion rate of Al^{z+} ions and explain the lower on-state resistance in the Pb-implanted device compared to the unimplanted device. It does not, however, explain why ToF-SIMS data in Figure 4 show Al penetrating further into the

GaLaSO layer in the unimplanted device, or why the Pb-implanted device has a higher set voltage than the unimplanted device. The surface modification of the GaLaSO film by Pb implantation could alter the interface with the Al top electrode so that it becomes more difficult initially to dissolve Al into the GaLaSO; this would explain the higher off-state resistance and set voltage in the Pb-implanted device. Once the Al is dissolved, it can be transported more easily because of the increased disorder. The SET voltages of our devices are over an order of magnitude higher than those observed in most other chalcogenide ECM cells—see Table I. The reduction potentials of Al, Ag, and Cu are -1.68 , 0.8 , and 0.34 V, respectively,²⁴ so it would also require a significantly greater electrode bias to reduce Al^{z+} ions into metal filaments than for Ag^{z+} or Cu^{z+} ions, which could explain the high set voltages in our devices. Table I also shows our Pb-implanted device has the highest resistance ratio and set voltage of chalcogenide-based resistive-switching devices.

In summary, we fabricated a resistive-switching device using an ITO inactive electrode, a GaLaSO solid-electrolyte, and an Al active electrode, with and without a 3×10^{15} ions/cm² Pb implantation before Al electrode deposition. The devices set at 2–3 and 3–4 V, with resistance ratios of 6×10^4 and 3×10^9 for the unimplanted and Pb-implanted devices, respectively, and no electroforming stage was required. The positive bias for switching showed that Al rather than ITO was the active electrode. The proposed mechanism of the set-reset behaviour was the electrochemical deposition and dissolution, respectively, of conductive Al metal filaments. In contrast to other chalcogenide-based resistive switching devices that use Ag or Cu as active electrodes, our devices reset at a positive, rather than negative, bias and had a significantly higher set voltage. We attribute this to the negative reduction potential of Al compared to the positive reduction potential of Ag and Cu, which would give Al metal filaments a propensity to oxidise. ToF-SIMS measurements showed that Al diffused 40 nm further into the GaLaSO layer in the unimplanted device compared to the Pb-implanted device. This was attributed to a physical barrier to ion diffusion caused by surface modification of the GaLaSO by ion implantation.

TABLE I. Chalcogenide-based resistive-switching device comparison.

Chalcogenide	Thickness (nm)	Active electrode	Set voltage (V)	Resistance ratio	References
Ge ₂ Sb ₂ Te ₅	29	Cu	0.6	2.5×10^3	6
N-doped Ge ₂ Sb ₂ Te ₅	29	Cu	2.7	1×10^7	6
Ge ₂₅ Se ₇₅	50	Ag	0.2	...	7
As ₂ S ₃	1000	Ag	0.25	1.5×10^4	8
Ge ₂₆ Se ₇₄	...	Ag	0.1	...	9
Ge ₃₀ Se ₇₀	60	Cu	0.2	160	10
GeTe	100	Cu	0.3	...	11
Ag ₂₀ Ge ₂₀ S ₆₀	30	Ag	0.62	1.9×10^4	12
Ga ₂₆ La ₁₂ S ₄₅ O ₁₇	215	Al	2–3	6×10^4	This work
Pb-implanted Ga ₂₆ La ₁₂ S ₄₅ O ₁₇	215	Al	3–4	3×10^9	This work

This work was supported by the UK EPSRC grants EP/I018414/1, EP/I019065/1, and EP/I018050/1. We would like to thank Dr. David Cox for taking the SEM cross section and assisting in its analysis. We would also like to thank Mr. Chris Craig for fabricating the GaLaSO sputtering target.

- ¹D. B. Strukov, G. S. Snider, D. R. Stewart, and R. S. Williams, *Nature* **453**(7191), 80–83 (2008).
- ²J. C. Scott and L. D. Bozano, *Adv. Mater.* **19**(11), 1452–1463 (2007).
- ³J. J. Yang, M. D. Pickett, X. M. Li, D. A. A. Ohlberg, D. R. Stewart, and R. S. Williams, *Nat. Nanotechnol.* **3**(7), 429–433 (2008).
- ⁴A. V. Kolobov and S. R. Elliott, *Adv. Phys.* **40**(5), 625–684 (1991).
- ⁵R. Waser, R. Dittmann, G. Staikov, and K. Szot, *Adv. Mater.* **21**(25–26), 2632–2663 (2009).
- ⁶S. Kim, J. Park, S. Jung, W. Lee, J. Woo, C. Cho, M. Siddik, J. Shin, S. Park, B. H. Lee, and H. Hwang, *Appl. Phys. Lett.* **99**(19), 192110 (2011).
- ⁷A. Pradel, N. Frolet, M. Ramonda, A. Piarristeguy, and M. Ribes, *Phys. Status Solidi A* **208**(10), 2303–2308 (2011).
- ⁸Y. Hirose and H. Hirose, *J. Appl. Phys.* **47**(6), 2767–2772 (1976).
- ⁹D. Reso, M. Silinskas, M. Lisker, A. Schubert, and E. P. Burte, *Appl. Phys. Lett.* **98**(15), 151901 (2011).
- ¹⁰R. Soni, P. Meuffels, A. Petraru, M. Weides, C. Kugeler, R. Waser, and H. Kohlstedt, *J. Appl. Phys.* **107**(2), 024517 (2010).
- ¹¹S.-J. Choi, G.-S. Park, K.-H. Kim, S. Cho, W.-Y. Yang, X.-S. Li, J.-H. Moon, K.-J. Lee, and K. Kim, *Adv. Mater.* **23**(29), 3272–3277 (2011).
- ¹²F. Wang, W. P. Dunn, M. Jain, C. De Leo, and N. Vickers, *Solid-State Electron.* **61**(1), 33–37 (2011).
- ¹³T. Yoshimasu, M. Akagi, N. Tanba, and S. Hara, *IEEE J. Solid-State Circuit* **33**(9), 1290–1296 (1998).
- ¹⁴Y. C. Yang, F. Pan, Q. Liu, M. Liu, and F. Zeng, *Nano Lett.* **9**(4), 1636–1643 (2009).
- ¹⁵M. J. Lee, Y. Park, D. S. Suh, E. H. Lee, S. Seo, D. C. Kim, R. Jung, B. S. Kang, S. E. Ahn, C. B. Lee, D. H. Seo, Y. K. Cha, I. K. Yoo, J. S. Kim, and B. H. Park, *Adv. Mater.* **19**(22), 3919–3923 (2007).
- ¹⁶A. Mehonic, S. Cuffeff, M. Wojdak, S. Hudziak, O. Jambois, C. Labbé, B. Garrido, R. Rizk, and A. J. Kenyon, *J. Appl. Phys.* **111**(7), 074507 (2012).
- ¹⁷Y. Li, Y. P. Zhong, L. Xu, J. J. Zhang, X. H. Xu, H. J. Sun, and X. S. Miao, *Sci. Rep.* **3**, 1619 (2013).
- ¹⁸M. A. Hughes, R. M. Gwilliam, K. Homewood, B. Gholipour, D. W. Hewak, T.-H. Lee, S. R. Elliott, T. Suzuki, Y. Ohishi, T. Kohoutek, and R. J. Curry, *Opt. Express* **21**(7), 8101–8115 (2013).
- ¹⁹M. A. Hughes, K. P. Homewood, R. J. Curry, Y. Ohno, and T. Mizutani, *Appl. Phys. Lett.* **103**(13), 133508 (2013).
- ²⁰S. J. Hinder, C. Lowe, and J. F. Watts, *Surf. Interface Anal.* **39**(6), 467–475 (2007).
- ²¹W. K. Njoroge, H.-W. Wöltgens, and M. Wuttig, *J. Vac. Sci. Technol. A* **20**(1), 230–233 (2002).
- ²²C. Ohly, S. Hoffmann-Eifert, X. Guo, J. Schubert, and R. Waser, *J. Am. Ceram. Soc.* **89**(9), 2845–2852 (2006).
- ²³K. Shibuya, R. Dittmann, S. Mi, and R. Waser, *Adv. Mater.* **22**(3), 411–414 (2010).
- ²⁴C. G. Zoski, *Handbook of Electrochemistry* (Elsevier, 2007).